Check for updates

Deployable Structures Based on Buckling of Curved Beams Upon a Rotational Input

Saurabh Mhatre, Elisa Boatti, David Melancon, Ahmad Zareei, Maxime Dupont, Martin Bechthold,* and Katia Bertoldi*

Inspired by the recent success of buckling-induced reconfigurable structures, a new class of deployable systems that harness buckling of curved beams upon a rotational input is proposed. First, experimental and numerical methods are combined to investigate the influence of the beam's geometric parameters on its non-linear response. Then, it is shown that a wide range of deployable architectures can be realized by combining curved beams. Finally, the proposed principles are used to build deployable furniture such as tables and lamp shades that are flat/compact for transportation and storage, require simple or no assembly, and can be expanded by applying a simple rotational input.

1. Introduction

From foldable chairs and umbrellas to architectural structures[1–4] and medical devices,[5] deployable structures that can be packaged for transportation and expanded at the time of operation are used to realize a wide range of transformable systems. While conventional designs are typically based on linkage mechanisms,[1–3,6–8] new deployment strategies have been recently proposed to transform compact planar structures into complex and diverse 3D geometries. Origami principles have been exploited for the realization of such systems.[9–19] Capillary forces have been harnessed to transform micro-scale 2D shapes into predetermined 3D structures.[20,21] Magnetic dipoles embedded into centimeter-sized flat sheets have enabled their folding into free-standing 3D objects.[22] Finally, mechanical instabilities in flat structures subjected to compressive stresses have been exploited to realize 3D architectures over a wide range of length scales.[23–30]

S. Mhatre, Prof. M. Bechthold
Harvard Graduate School of Design
Harvard University
Cambridge, MA 02138, USA
E-mail: mbechthold@gsd.harvard.edu
Dr. E. Boatti, D. Melancon, Dr. A. Zareei, M. Dupont, Prof. K. Bertoldi
Harvard John A. Paulson School of Engineering and Applied Sciences
Harvard University
Cambridge, MA 02138, USA
E-mail: bertoldi@seas.harvard.edu
Prof. K. Bertoldi
Kavli Institute
Harvard University
Cambridge, MA 02138, USA

The ORCID identification number(s) for the author(s) of this article can be found under https://doi.org/10.1002/adfm.202101144.

Inspired by the recent success of buckling-induced reconfigurable structures, we propose a new family of deployable systems that harness mechanical instabilities in curved beams to attain elaborate and customizable 3D configurations. While most of the previously proposed buckling-induced deployable structures are activated by compressive forces,[23–30] our systems relies on a rotational movement to induce buckling as the trigger for the 2D to 3D transformation. We first use a combination of experiments and numerical analyses to investigate the influence of the geometrical parameters on the final deployed configuration. Then, we demonstrate the potential of the proposed strategy for the development of complex pop-up architectures and compact deployable furniture.
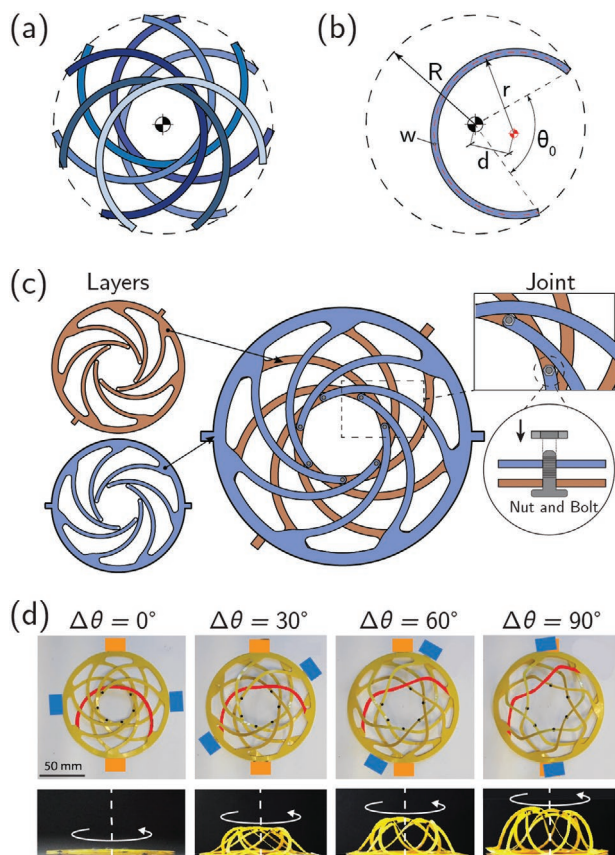
2. Deployable Structures Based on Curved Elastic Beams

All our deployable structures comprise of a circular array of initially flat elastic beams with constant in-plane curvature $1/r$ and rectangular cross-section $t \times w$ (see **Figure 1**a). To begin with, we consider circular beams with opening angle θ_0 and ends constrained to move along a circular guiding path with radius R and center located at a distance d from that of the beams (see Figure 1b). As a representative example, in Figure 1c,d we focus on a system composed of 7 curved beams with $t/w = 0.1$, $w/R = 0.067$, $d/R = 0.4$ and $\theta_0 = 110°$. The structure is realized at the centimeter-scale by i) laser cutting two copies of the part shown in Figure 1c from polyethylene terephthalate glycol (PETG) plastic shims (with thickness $t \simeq 0.5$ mm); ii) flipping and rotating by 90° one of the parts and overlapping the two; iii) joining each pair of protruding half-length curved beams with miniaturized bolts to form seven full-length beams (Figure 1c). The result is a circular pattern of curved beams, each presenting one end connected to the top layer (blue) and one end to the bottom layer (orange) (Figure S1, Supporting Information). Notably, deployment of this structure can be achieved by simply applying an in-plane relative rotation between the two layers (Movie S1, Supporting Information). More specifically, as presented in Figure 1d, a transformation from the initial 2D configuration to a complex 3D geometry is triggered by rotating the top layer (blue handles) by $\Delta\theta$ with respect to the bottom layer (orange handles). Focusing on an individual curved beam (highlighted in red in Figure 1d),

**ADVANCED
SCIENCE NEWS**
www.advancedsciencenews.com

**ADVANCED
FUNCTIONAL
MATERIALS**
www.afm-journal.de

Figure 1. Deployable structures based on buckling of curved beams upon a rotational input. a) Schematics of a representative structure. b) Schematics of a circular beam. c) Schematics illustrating the assembly process. d) Snapshots of a structure comprising seven curved beams with $(t/w, w/R, d/R, \theta_0) = (0.1, 0.067, 0.4, 100°)$ at different levels of rotational input $\Delta\theta$. Both top view (top) and side view (bottom) are shown.

we find that the applied rotation $\Delta\theta$ further separates its two ends, increasing its opening angle from the initial value θ_0 to a larger value θ. At a critical opening angle, θ_{cr}, the initially flat beam buckles out-of-plane and the structure transforms into a 3D configuration.

To better understand the mechanism resulting in the deployment of the structure, we consider a single beam identical to those embedded in the structure of Figure 1, with ends fixed to move on a circle of radius R, and progressively increase its opening angle θ. As shown in **Figure 2**a, we find that at $\Delta\theta_{cr} \approx 3.6°$ the beam buckles out-of plane and transforms into a 3D shape similar to that observed in the structure of Figure 1. However, it is important to note that not all curved beam geometries exhibit such upward buckled configuration. As an example, in Figure 2b we report snapshots for a beam with the same geometrical dimensions as the previous one, except for θ_0 which this time is set to 30°. While the displacement applied at its ends still triggers out-of-plane deformation, this time the beam buckling is not unidirectional; about half of the beam buckles upward and half downward. Therefore, these preliminary tests demonstrate that the geometrical parameters have a major influence on beam buckling and can be used to target specific deployed shapes.

3. Numerical Analysis

To better understand the effect of the geometry of the beams on the buckling mode, we analyze the deformation of our building block using finite element (FE) analyses. In our simulations (conducted using the commercial package ABAQUS 2019/Standard), we discretize the beams with four-node shell elements (ABAQUS element type: S4R), and use a linear elastic material model with Young's modulus $E = 2$ GPa and Poisson's ratio $\nu = 0.4$. To simulate the experiments, we clamp one edge of the beam and apply a rotation $\Delta\theta$ to the other end using a reference point at the origin and coupling constraint (ABAQUS constraint type: Kinematic coupling). First, we perform a linear buckling analysis to extract the critical angle θ_{cr} and the corresponding buckling mode. We then apply a small imperfection to the mesh in the form of this buckling mode and simulate the nonlinear buckling using the arc-length method (ABAQUS step type: Static-Riks). Note that, while in all our simulations we assume the beams to be at room temperature and we do not consider loads applied to the deployed configuration, the numerical analyses can also be extended to investigate the effect of both temperature and external forces on their mechanical response (Figures S11 and S12, Supporting Information).

To test the validity of our analyses, we compare the numerically predicted deformed configurations to the experimentally observed ones for a variety of beams. The snapshots of the progressively deformed beams reported in Figure 2a,b show that the simulations correctly capture the effect of geometric parameters and confirm that by controlling the geometry we can tune the characteristic of the buckling mode and trigger either unidirectional (i.e., only upward) or bi-directional (i.e., both upward and downward) deformations. Further, the simulations also indicate that the maximum out-of-plane displacement along the z-axis, u_z^{max}, is much higher when the beam buckles into a unidirectional mode (see Figure 2d). Since in this study we are interested in exploiting beam buckling to realize deployable systems, in the remainder of this article we will focus on configurations that buckle unidirectionally.

Having confirmed the validity of our analyses, we next use them to get a deeper understanding of the impact of geometric parameters on the response of the beams. Toward this end, in **Figure 3** we report the evolution of the normalized critical angle, $\tilde{\theta}_{cr} = (\theta_{cr} - \theta_0)/(2\pi - \theta_0)$ as a function of different combinations of geometric parameters highlighted in Figure 3a. As shown in Figure 3b, for beams with $d/R = 0.4$ and $w/R = 0.067$, we find that θ_0 has a strong influence on the characteristics of the critical buckling mode. While for low values of θ_0 the beams exhibit a bidirectional buckling modes (shaded region in Figure 3b), above a critical value of θ_0 such buckling modes become unidirectional. Further, our results indicate that within the unidirectional buckling region t/w has the greatest effect on the critical buckling angle, with $\tilde{\theta}_{cr}$ always monotonically increasing with t/w (see Figure 3b–d). By contrast, for the sets of parameters considered in Figure 3 the normalized critical angle $\tilde{\theta}_{cr}$ is almost unaltered by variations in w/R.

In Figure 3 we have focused on the out-of-plane behavior of circular beams. However, it is important to point out that
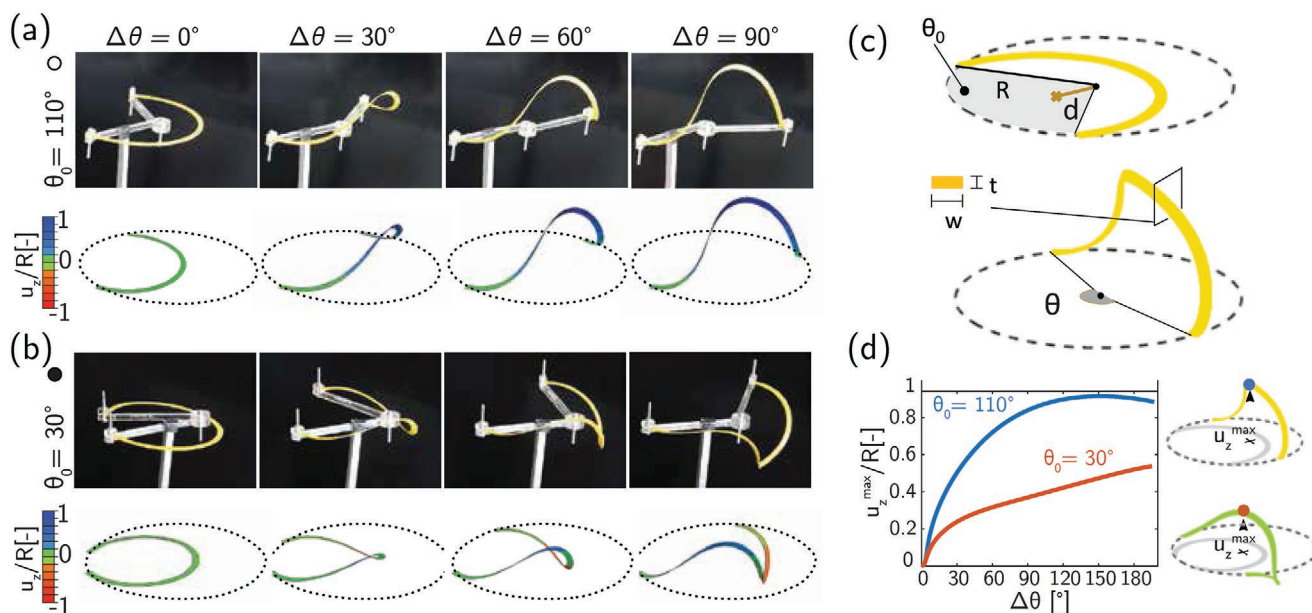
Figure 2. Buckling of curved circular beams. Experimental (top) and numerical (bottom) snapshots of curved beams with $t/w = 0.1$, $w/R = 0.067$, $d/R = 0.4$ and a) $\theta_0 = 110°$ and b) $\theta_0 = 30°$ for different levels of applied rotation $\Delta\theta$. c) Schematic diagram of a beam with all relevant parameters, in both initial (top) and buckled (bottom) configurations. The guiding circle is represented by a black dashed line. d) Numerically predicted evolution of the maximum out-of-plane displacement u_z^{max} as a function of $\Delta\theta$ for the two beams considered in (a) and (b).

our numerical approach can be extended to investigate beams of arbitrary shape. As an example, in **Figure 4** we consider a double arc beam based on the intersection of two circular ones (Figure 4a) and use FE simulations to explore the effect of the geometric parameters on its response upon application of a rotational input. The results reported in Figure 4b,c indicate that also for double arc beams the critical buckling angle $\tilde{\theta}_{cr}$ is only moderately affected by w/R and the opening angle θ_1. However, differently from the case of the circular beams, we find that buckling always leads to unidirectional out-of-plane deformation.
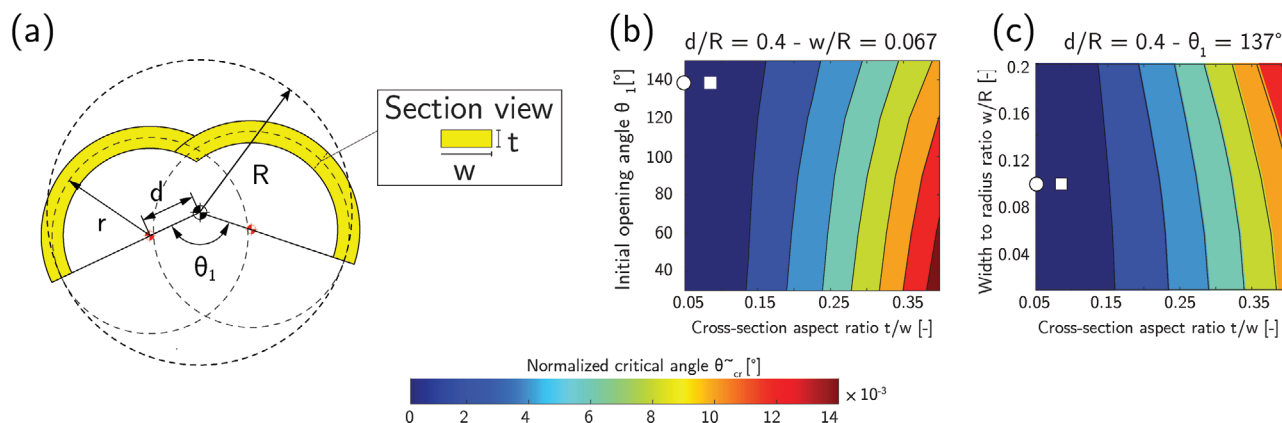
4. Programmable and Deployable Architectures

Having investigated the effect of the beam geometry on buckling, we now proceed to realize deployable architectures by combining different circular beams on a simple turntable (McMaster Part No. 1797K12) to which we apply a rotation. To begin with, we focus on four identical beams with $(w/R, t/w, d/R, \theta_0) = (0.054, 0.15, 0.15, 140°)$ (see triangular marker in Figure 3c), arrange them in a circular array and connect one of their ends to the static part of the turntable and the other one to the rotating part (see **Figure 5** and Figure S3,
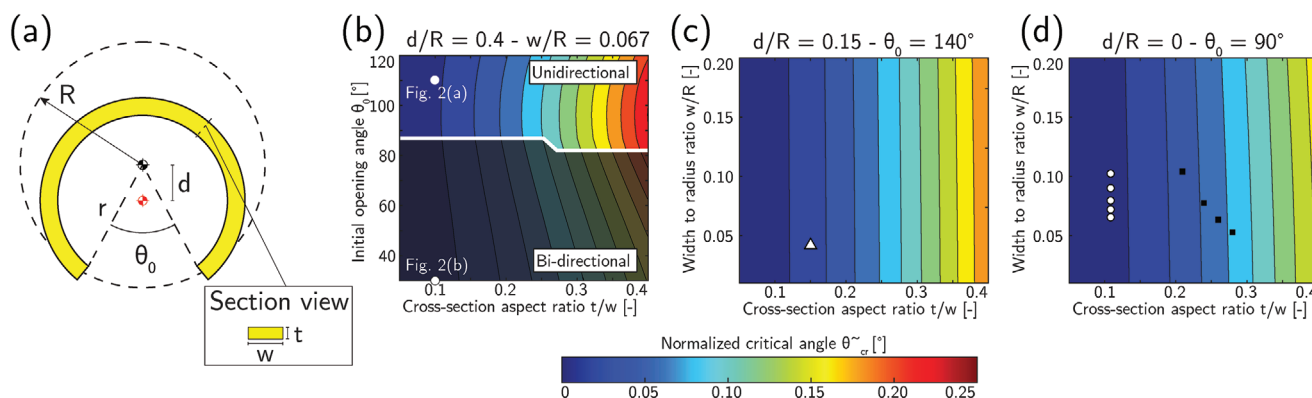

Figure 3. Effect of the geometry of the beam on the critical angle $\tilde{\theta}_{cr}$ for circular beams. a) Schematic diagram of a circular beam in its initial/flat configuration with all relevant geometric parameters. b–d) Numerically predicted evolution of $\tilde{\theta}_{cr}$ for beams with b) $d/R = 0.4$, $w/R = 0.67$, $t/w \in [0.05, 0.4]$, and $\theta_0 \in [35°, 120°]$; c) $d/R = 0.15$, $\theta_0 = 140°$, $t/w \in [0.05, 0.4]$, and $w/R \in [0.01, 0.20]$; d) $d/R = 0$, $\theta_0 = 90°$, $t/w \in [0.05, 0.4]$, and $w/R \in [0.01, 0.20]$. The shaded area in (b) corresponds to the region where the unwanted bi-directional buckling mode arises. The circular markers in (b) identify the geometries considered in Figure 2. The triangular marker in (c) identifies the geometries considered in Figure 5. The circular and square markers in (d) identify the geometry of the beams composing the structures considered in Figure 6.

**ADVANCED
SCIENCE NEWS**

www.advancedsciencenews.com

**ADVANCED
FUNCTIONAL
MATERIALS**

www.afm-journal.de

Figure 4. Effect of the geometry of the beam on the critical angle $\tilde{\theta}_{cr}$ for double arc beams. a) Schematic diagram of an double arc beam in its initial/flat configuration with all relevant geometric parameters. b–c) Numerically predicted evolution of $\tilde{\theta}_{cr}$ for beams with b) $d/R = 0.4$, $w/R = 0.67$, $t/w \in [0.05, 0.4]$, and $\theta_0 \in [35°, 150°]$; c) $d/R = 0.4$, $\theta_0 = 137°$, $t/w \in [0.05, 0.4]$, and $w/R \in [0.01, 0.20]$. The circular and square markers identify the geometry of the beams composing the structures considered in Figures 7 and 8, respectively.

Supporting Information). As shown in Figure 5, a large enough rotation imposed to the turntable produces the simultaneous buckling of the four beams and leads to the formation of a 3D dome-like form. Differently, if we arrange the beams concentrically the buckling induced pop-up of the strips results in a 3D wave-like configuration (**Figure 6**a). Note that the deployment sequence for these architectures can be easily programmed using the results of Figure 3d. When choosing five beams with identical cross-sectional aspect ratio (white circular markers in Figure 3d), buckling induces the simultaneous pop-up of all strips (Figure 6a), since $\tilde{\theta}_{cr}$ is identical for all elements. Differently, if the beams have different t/w ratios and, therefore, different $\tilde{\theta}_{cr}$ (black square markers in Figure 3d) the pop-up process is sequential, with the thinnest beam that buckles first and the thickest one that buckles last (Figure 6b—see also Figure S4 and Movie S3, Supporting Information). We also find that the deformation of all considered architectures is nicely captured when combining the FE results obtained for the individual beams (see numerical snapshots in Figures 5 and 6). Since the numerical results do not account for friction and contact, a good agreement between simulations and experiments clearly indicates that the response of the architectures is fully dictated by the geometry of the beams.
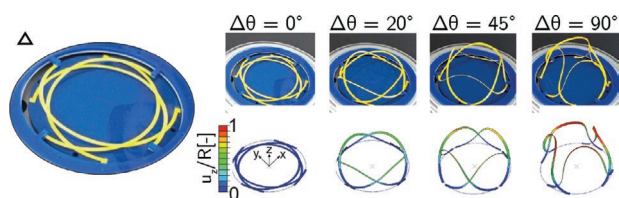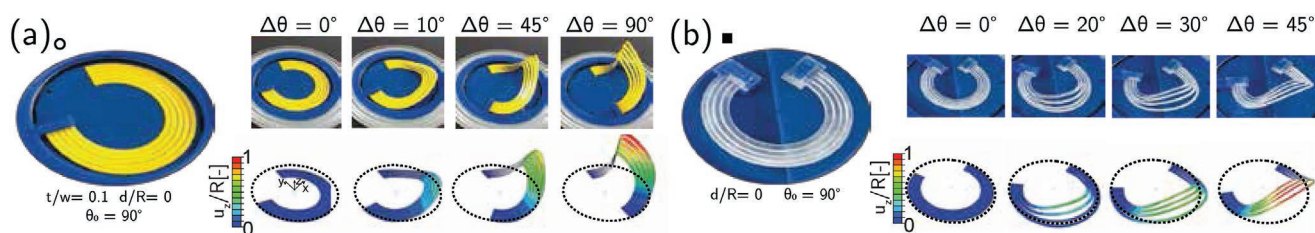

Figure 5. Four identical beams with $(w/R, t/w, d/R, \theta_0) = (0.054, 0.15, 0.15, 140°)$ arranged in a circular array. Experimental (top) and numerical (bottom) snapshots for different rotational inputs. Since the beams are identical, they all buckle simultaneously forming a 3D dome-like pattern.

5. Deployable Furniture

So far we have shown that a variety of 3D architectures can be obtained by harnessing mechanical instabilities in curved beams upon a rotational input. Although we have demonstrated the concept at the centimeter scale, it is important to point out that our approach can be extended to design deployable structures over a wide range of length scales. In this paper we focus on deployable furniture and use the proposed principles to realize tables and lamp shades that are flat/compact for transportation and storage, require simple or no-assembly, and can be expanded by applying a simple rotational input.

As a first prototype we designed a human-scale, plastic coffee table by arranging in a circular array ten double arc beams with $w/R = 0.1$, $t/w = 0.068$, $d/R = 0.4$, $\theta_1 = 137°$ and $R = 440.25$ mm (square markers in Figure 4b,c). The table is realized by computer numerical control (CNC) cutting 4.76 mm-thick PETG plastic sheets to form the two layers shown in **Figure 7**a as well as a circular disc with a diameter of 1.14 m. Note that the disc is rigidly attached to the perimeter of the top layer, and that the other two layers of beams are connected by joining the ends of the converging beams with rivets (Figure S5, Supporting Information). The table is then deployed by rotating the two layers of beams relatively to each other using the designed tabs (Figure 7b) and also in this case we find excellent agreement between experiments and simulations (Figure 7c). Finally the table is locked in place with two pairs of nuts and bolts (see Figure S5 and Movie S4, Supporting Information). In the deployed state the circular disc acts as the table top, whereas the beams layers act as its legs (Figure 7d). Note that our prototype in its deployed configuration has an height of 35 cm, closely matching the height of 36.4 cm predicted by our FE analyses. Finally, we want to point out that our deployable table can be deployed in under 1 min, is capable of carrying up to 7 kg and can be made even more stable by adding a central tie and introducing self locking tabs (Figure S7, Supporting Information).

Figure 6. Two different sets of beams arranged concentrically. a) Structure comprising five beams with $(t/w, d/R, \theta_0) = (0.1, 0, 90°)$ and $w/R = (0.118, 0.105, 0.094, 0.086, 0.079)$ (from inside to outside). b) Structure comprising four beams with $(d/R, \theta_0) = (0, 90°)$ and $t/w = (0.2, 0.23, 0.25, 0.27)$ (from inside to outside) and $w/R = (0.120, 0.092, 0.077, 0.066)$ (from inside to outside). Experimental (top) and numerical (bottom) snapshots for different rotational inputs are reported on the right.

Next, we exploit the buckling of curved beams to realize a tunable lamp shade. Since circular arrays of curved beams with constant width exhibit large voids in both the flat and the expanded configuration (see Figures S9a–c, Supporting Information), we modify the profile of the beams to minimize the void area fraction in the flat state (see Figure S9e, Supporting Information). Specifically, we start with an array of 16 double arc beams with $w/R = 0.1$, $t/w = 0.05$, $d/R = 0.4$, $\theta_1 = 137°$ and $R = 99.26$ mm (circular markers in Figure 4b,c). Then, we design the profile of each beam such that its outer circular edge is extended to match exactly the inner circular edge of the next beam (see **Figure 8**a), resulting in a geometry without void in the initial/flat state. To fabricate the lamp shade, we embed a chiral pattern comprising 16 curved cuts (each) into two disc made of 0.5 mm-thick PETG (Figure 8b). We then rigidly connect the two layers at the center using rivets to form 16 double arc beams with varying cross-section. While the resulting structure is fully closed in its flat state, it becomes increasingly more porous as it is deployed by imposing a simple relative rotation between the two layers (see experimental and FE snapshots in Figure 8c,d). Hence, when a light source is placed behind it, the deployment process can be exploited to control the amount of light emitted to the environment (see Movie S5, Supporting Information). While our prototype requires an external light, we believe that by manufacturing similar designs out of flexible electroluminescent sheets, structures can be realized that emit light without relying on an integrated light source (see Figure S9f, Supporting Information). As such, our simple yet effective system, with its high parametric flexibility and the abil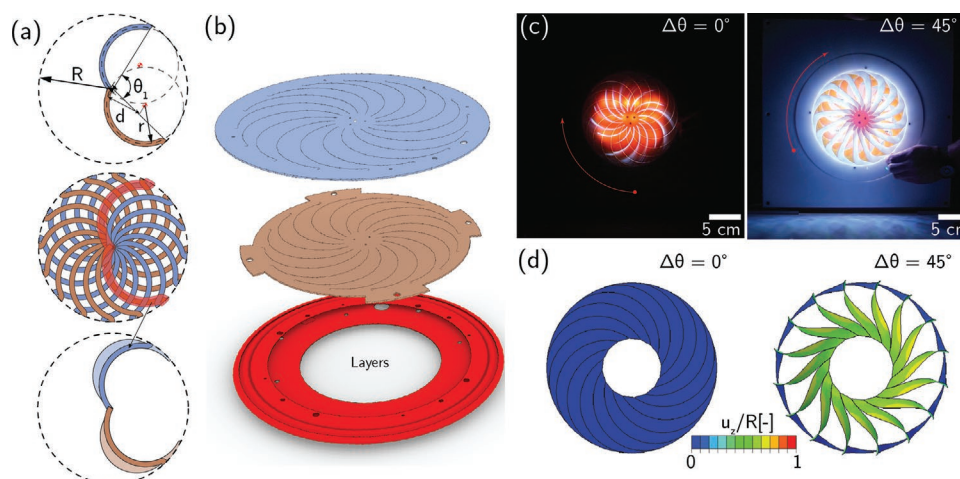ity to be realized with a variety of smart sheet materials, holds promise to greatly expand the application space of deployable furniture.

6. Conclusions

To summarize, we have proposed a new platform for the design of deployable structures based on the buckling of curved, slender beams upon a rotational input. We have shown that by carefully choosing the beam's geometrical parameters and their arrangement a vast range of diverse 3D configurations and deployment sequences can be realized. While initially we have focused on desktop-scale prototypes, we have then shown that the proposed strategy can be used to realize deployable furniture that can be expanded by applying a simple rotational input. Importantly, our idea can be extended to realize functional structures and devices over a wide range of scales and out of a variety of different materials. For example, millimeter scale metallic deployable devices can be built using the pop up laminate method[31] (see Figure S10 and Movie S6, Supporting Information), whereas meter-scale architectures made out of plastics and metals can be fabricated using CNC cutting techniques. Finally, the concept can be combined with additional technologies such as flexible electronics and smart films like dichroic films, light redirection films, and polarizing films to further expand its capabilities. As such, we envision the proposed platform to provide opportunities for a generation of functional deployable systems that are low weight, compact, inexpensive, easy to manufacture, and can be easily designed to satisfy different requirements and provide a wide range of functionalities.
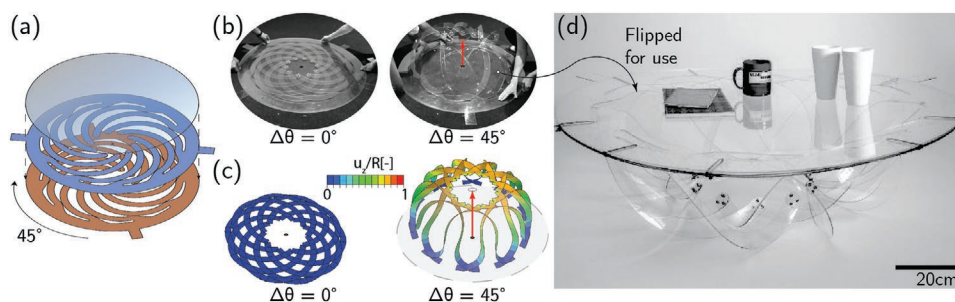
Figure 7. Deployable coffee table. a) Schematics showing the parts of the table. b) Experimental snapshots showing the table in its initial and deployed state. c) Numerical snapshots showing the table in its initial and deployed state. d) Experimental snapshot showing the table in use.

**ADVANCED
SCIENCE NEWS**

www.advancedsciencenews.com

**ADVANCED
FUNCTIONAL
MATERIALS**

www.afm-journal.de

Figure 8. Tunable lamp shape. a) Schematics showing the modification of the double arc beam width to reduce the void area fraction in the initial configuration. b) Schematics showing the parts of the lamp shade. c) Experimental snapshots showing the lamp shade in its initial and deployed state. d) Numerical snapshots showing the lamp shade in its initial and deployed state.

7. Experimental Section

Details of fabrication of the proposed deployable structures are described in Section S1, Supporting Information. Additional numerical results are reported in Section 2.

Supporting Information

Supporting Information is available from the Wiley Online Library or from the author.

Conflict of Interest

The authors declare no conflict of interest.

Data Availability Statement

Data sharing is not applicable to this article as no new data were created or analyzed in this study.

[1] T. Ziegler, US3968808A, **1976**.
[2] C. Hoberman, US5024031A, **1991**.
[3] P. Kassabian, Z. You, S. Pellegrino, *Proc. Inst. Civil Eng. Struct. Bldg.* **1999**, *134*, 45.
[4] C. Gantes, J. Connor, R. Logcher, Y. Rosenfield, *Comput. Struct.* **1989**, *32*, 661.
[5] Stoeckel, Bonsignore, Duda, Minimally Invasive Ther. Allied Technol. 2002, 11, 137.
[6] A. Britt, H. Lalvani, in *IUTAM-IASS Symposium on Deployable Structures: Theory and Applications*, Springer, Berlin, Heidelberg **1998**, pp. 45–54.
[7] F. V. Jensen, S. Pellegrino, *J. Int. Assoc. Shell Spatial Struct.* **2005**, *46*, 151.
[8] Z. You, Y. Chen, *P. R. Soc. A* **2008**, *464*, 1275.
[9] K. Miura, *Inst. Space Astronaut. Sci. Rep.* **1985**, *618*, 1.
[10] G. Hunt, I. Ario, *Int. J. Non-Linear Mech.* **2005**, *40*, 833.
[11] E. Hawkes, B. An, N. M. Benbernou, H. Tanaka, S. Kima, E. D. Demaine, D. Rus, R. Wood, *Proc. Natl. Acad. Sci. U. S. A.* **2010**, *107*, 12441.
[12] S. Zirbel, R. Lang, M. Thomson, D. Sigel, P. Walkemeyer, B. Trease, S. Magleby, L. Howell, *J. Mech. Design* **2013**, *135*, 11.
[13] M. Tolley, S. Felton, S. Miyashita, D. Aukes, D. Rus, R. Wood, *Smart Mater. Struct.* **2014**, *23*, 9.
[14] J. L. Silverberg, A. A. Evans, L. Mcleod, R. C. Hayward, T. Hull, C. D. Santangelo, I. Cohen, *Science* **2014**, *345*, 647.
[15] S. Felton, M. Tolley, E. Demaine, D. Rus, R. Wood, *Science* **2014**, *345*, 6197644.
[16] A. Viquerat, M. Schenk, B. Sanders, V. J. Lappas, in *European Conf. on Spacecraft Structures, Materials and Environmental Testing*, ESA Publications, Washington, D.C **2014**, pp. 1–10.
[17] E. T. Filipov, T. Tachi, G. H. Paulino, *Proc. Natl. Acad. Sci. U. S. A.* **2015**, *112*, 12321.
[18] J. T. B. Overvelde, J. C. Weaver, C. Hoberman, K. Bertoldi, *Nature* **2017**, *541*, 347.
[19] N. Nayakanti, S. Tawfick, A. Hart, *Extreme Mech. Le.* **2018**, *21*, 17.
[20] R. R. A. Syms, E. M. Yeatman, V. M. Bright, G. M. Whitesides, *J. Microelectromech. Syst.* **2003**, *12*, 387.
[21] C. Py, P. Reverdy, L. Doppler, J. Bico, B. Roman, C. N. Baroud, *Phys. Rev. Lett.* **2007**, *98*, 156103.
[22] M. Boncheva, S. Andreev, L. Mahadevan, A. Winkleman, D. R. Reichman, M. G. Prentiss, S. Whitesides, G. M. Whitesides, *Proc. Natl. Acad. Sci. U. S. A.* **2005**, *102*, 3924.

[23] V. Y. Prinz, D. Gruetzmacher, A. Beyer, C. David, B. Ketterer, *Nanotechnology* **2001**, *12*, 399.

[24] J. Kim, J. A. Hanna, M. Byun, C. D. Santangelo, R. C. Hayward, *Science* **2012**, *335*, 1201.

[25] S. Xu, Z. Yan, K.-I. Jang, W. Huang, H. Fu, J. Kim, Z. Wei, M. Flavin, J. McCracken, R. Wang, A. Badea, Y. Liu, D. Xiao, G. Zhou, J. Lee, H. U. Chung, H. Cheng, W. Ren, A. Banks, X. Li, U. Paik, R. G. Nuzzo, Y. Huang, Y. Zhang, J. A. Rogers, *Science* **2015**, *347*, 154.

[26] Y. Zhang, Z. Yan, K. Nan, D. Xiao, Y. Liu, H. Luan, H. Fu, X. Wang, Q. Yang, J. Wang, W. Ren, H. Si, F. Liu, L. Yang, H. Li, J. Wang, X. Guo, H. Luo, L. Wang, Y. Huang, J. A. Rogers, *Proc. Natl. Acad. Sci. U. S. A.* **2015**, *112*, 11757.

[27] Z. Yan, F. Zhang, J. Wang, F. Liu, X. Guo, K. Nan, Q. Lin, M. Gao, D. Xiao, Y. Shi, Y. Qiu, H. Luan, J. H. Kim, Y. Wang, H. Luo, M. Han, Y. Huang, Y. Zhang, J. A. Rogers, *Adv. Funct. Mater.* **2016**, *26*, 2629.

[28] K.-I. Jang, H. U. Chung, S. Xu, H. N. Jung, Y. Yang, J. W. Kwak, H. H. Jung, J. Song, C. Yang, A. Wang, Z. Liu, J. Y. Lee, B. H. Kim, J.-H. Kim, J. Lee, Y. Yu, B. J. Kim, H. Jang, K. J. Yu, J. Kim, J. W. Lee, J.-W. Jeong, Y. M. Song, Y. Huang, Y. Zhang, J. A. Rogers, *Nat. Commun. 2017* **2017**, *8*, 15894.

[29] H. Fu, K. Nan, P. Froeter, W. Huang, Y. Liu, Y. Wang, J. Wang, Z. Yan, H. Luan, X. Guo, Y. J. Zhang, C. Jiang, L. Li, A. C. Dunn, X. Li, Y. Huang, Y. H. Zhang, J. A. Rogers, *Small* **2017**, *13*, 1700151.

[30] H. Zhao, K. Li, M. Han, F. Zhu, A. Vázquez-Guardado, P. Guo, Z. Xie, Y. Park, L. Chen, X. Wang, H. Luan, Y. Yang, H. Wang, C. Liang, Y. Xue, R. D. Schaller, D. Chanda, Y. Huang, Y. Zhang, J. A. Rogers, *Proc. Natl. Acad. Sci. U. S. A.* **2019**, *116*, 13239.

[31] D. M. Aukes, B. Goldberg, M. R. Cutkosky, R. J. Wood, *Smart Mater. Struct.* **2014**, *23*, 9.

ADVANCED FUNCTIONAL MATERIALS

Supporting Information

Deployable Structures Based on Buckling of Curved Beams Upon a Rotational Input

Saurabh Mhatre, Elisa Boatti, David Melancon, Ahmad Zareei, Maxime Dupont, Martin Bechthold,* and Katia Bertoldi*

Supplementary Materials

Deployable structures based on buckling of curved beams upon a rotational input

Saurabh Mhatre, Elisa Boatti, David Melancon, Ahmad Zareei, Maxime Dupont, Martin Bechthold, Katia Bertoldi

This PDF file includes:

Figs. S1 to S12
References for SI reference citations

S1. Fabrication and testing

In this Section we provide details on the fabrication of the structures reported in the main text as well as on their deployment.

A. Structure considered in Fig. 1. The structure considered in Fig. 1 of the main text can be fabricated using the following 3 steps:

1. Laser cut the two parts shown in Fig. S1a from 0.002" PETG plastic. We used a 150W Universal Laser and set Power to 80% and Speed to 4%.

2. Flip and rotate one of the parts by 90° and overlap it with the other.

3. Join each pair of half-length curved beams with nylon bolts (M2 size) to form 7 full-length beams.

The resulting structure comprises 7 curved beams (characterized by $t/w= 0.1$, $w/R= 0.067$, $d/R= 0.4$ and $\theta_0= 110°$) and actuation tabs connected to each layer (see Fig. S1b). It can be deployed by fixing the tabs connected to the upper layer and by applying an in-plane relative rotation (clockwise) to the tabs connected to the lower layer until all the beams buckle (see Fig. S1c).
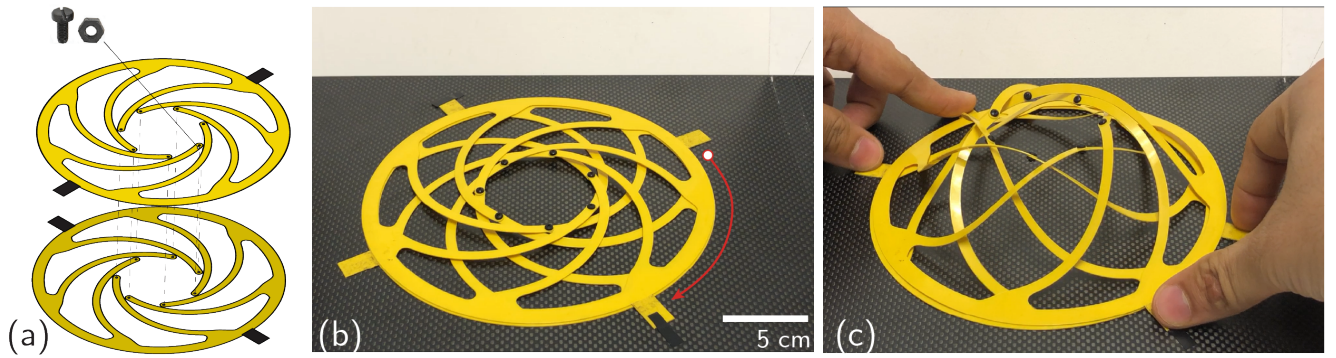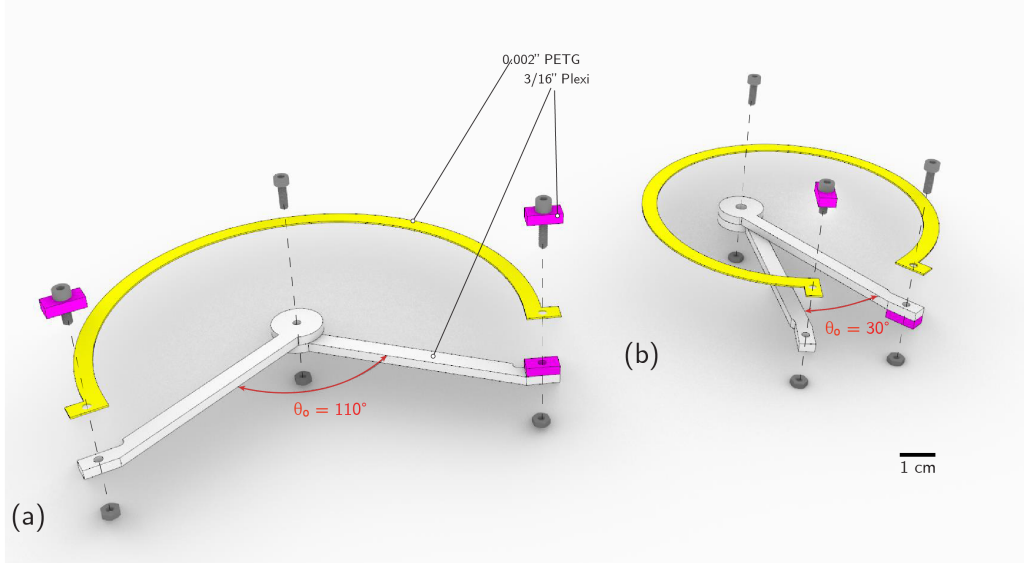

Fig. S1. Structure considered in Fig. 1. (a) Schematics showing its two parts. (b) Snapshot of the structure in its flat configuration. (c) Snapshot of the structure in its deployed configuration.

B. Structures considered in Fig. 2. The structures considered in Fig. 2 of the main text can be fabricated using the following 2 steps:

1. Laser cut the beams from 0.002" PETG plastic.

2. Attach the beams to a 3/16" acrylic armature with the help of bolts and rectangular washers (see Fig. S2).

The beams are deployed by progressively increasing the opening angle θ until the beams buckle.
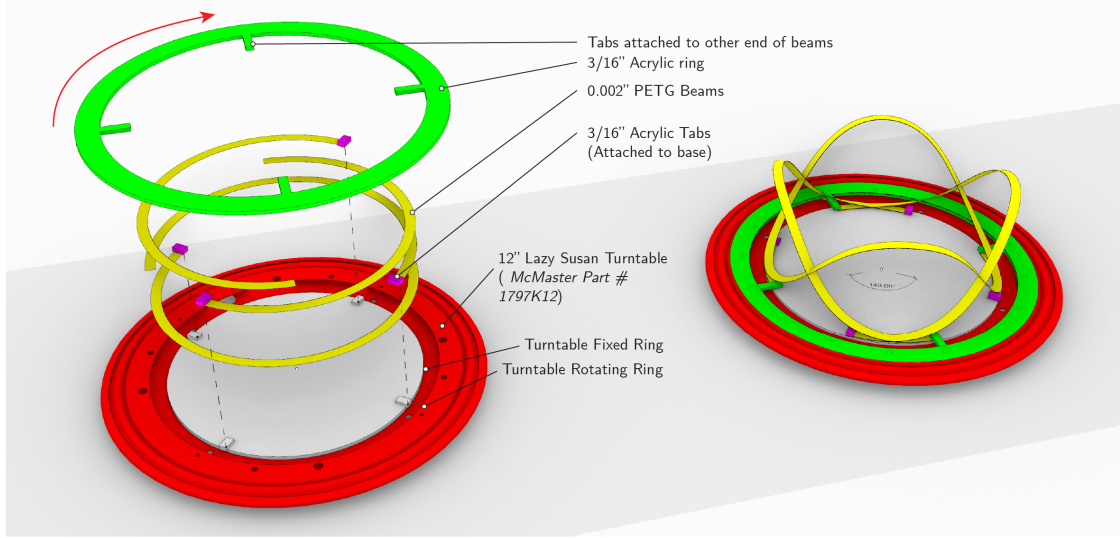

Fig. S2. Schematics of the structure considered in Fig. 2. Schematics of assembly of curved beam with with t/w=0.1, $w/R = 0.067$, $d/R = 0.4$ and (a) $\theta_0 = 110°$ and (b) $\theta_0 = 30°$

C. Structure considered in Fig. 5. The structure considered in Fig. 5 of the main text can be fabricated using the following 3 steps:

1. Laser cut 4 beams from 0.002" PETG plastic sheets. The beams are characterized by $(w/R,\ t/w,\ r/R,\ \theta_0) = (0.054,\ 0.15,\ 0.15,\ 140°)$

2. Attach one end of each beam to a 3/16" acrylic ring (shown in green in Fig. S3) with the help of bolts and rectangular washers.

3. Attach the other end of each beam to the fixed ring of a turntable (McMaster Part No.1797K12) (shown in red in Fig. S3) with the help of bolts and rectangular washers.

To deploy the structure, we rotate the acrylic ring (attached to the rotating ring of the turntable) clockwise while keeping the base of the turntable fixed. This causes the 4 beams to buckle simultaneously.
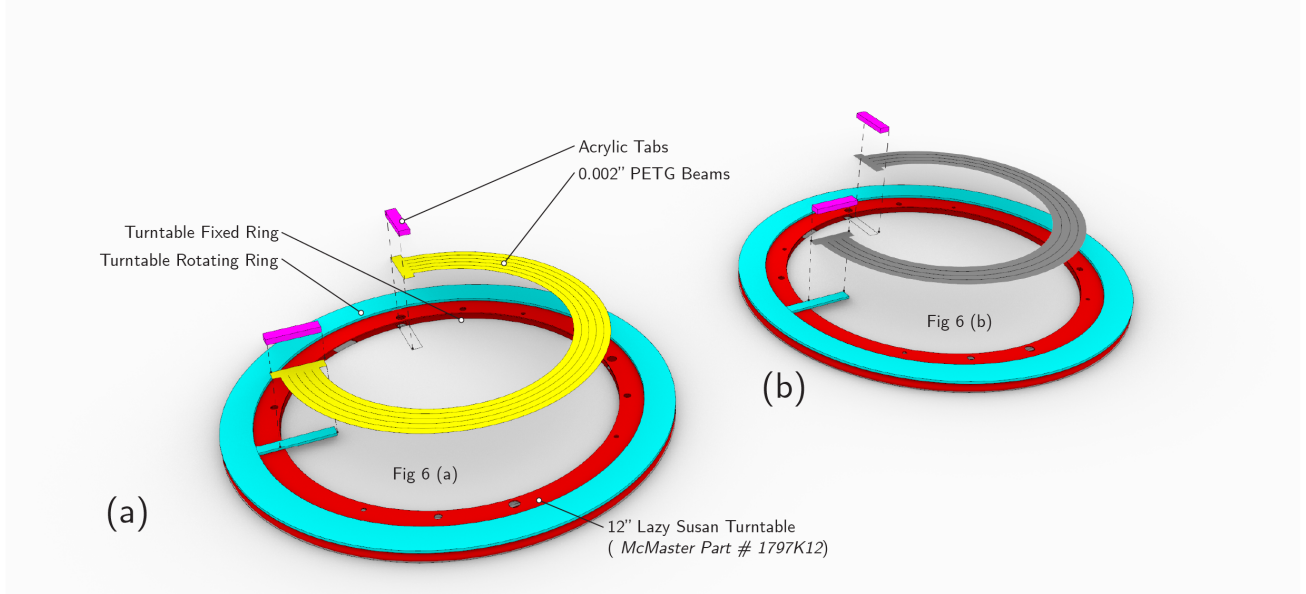

Fig. S3. Schematics of the structure considered in Fig. 5.

D. Structures considered in Fig. 6. The structures considered in Fig. 6 of the main text can be fabricated using the following 2 steps:

1. The 2 sets of concentric 4 beams, one with identical cross-section and the other one with varying cross-section, are laser cut from 0.002" PETG plastic sheets. Note that their ends merge on a single piece as shown in Fig. S4a.

2. One end of the beams is connected to the static part of the turntable (shown in red in Fig. S4) and the other to its rotating part (shown in blue in Fig. S4) using bolts and rectangular washers.

The beams are deployed by rotating in anti-clockwise direction the ring shown in blue in Fig. S4, while keeping the other ring (shown in red in Fig. S4) fixed.

Fig. S4. Schematics of the structure considered in Fig. 6. (a) Schematics of structure comprising 5 beams with $(t/w, d/R, \theta_0)$=(0.1, 0, 90°) and $w/R = (0.118, 0.105, 0.094, 0.086, 0.079)$ (from inside to outside). (b) Schematics of structure comprising 4 beams with $(d/R, \theta_0)$=(0, 90°) and $t/w = (0.2, 0.23, 0.25, 0.27$)(from inside to outside) and $w/R = (0.120, 0.092, 0.077, 0.066)$ (from inside to outside)
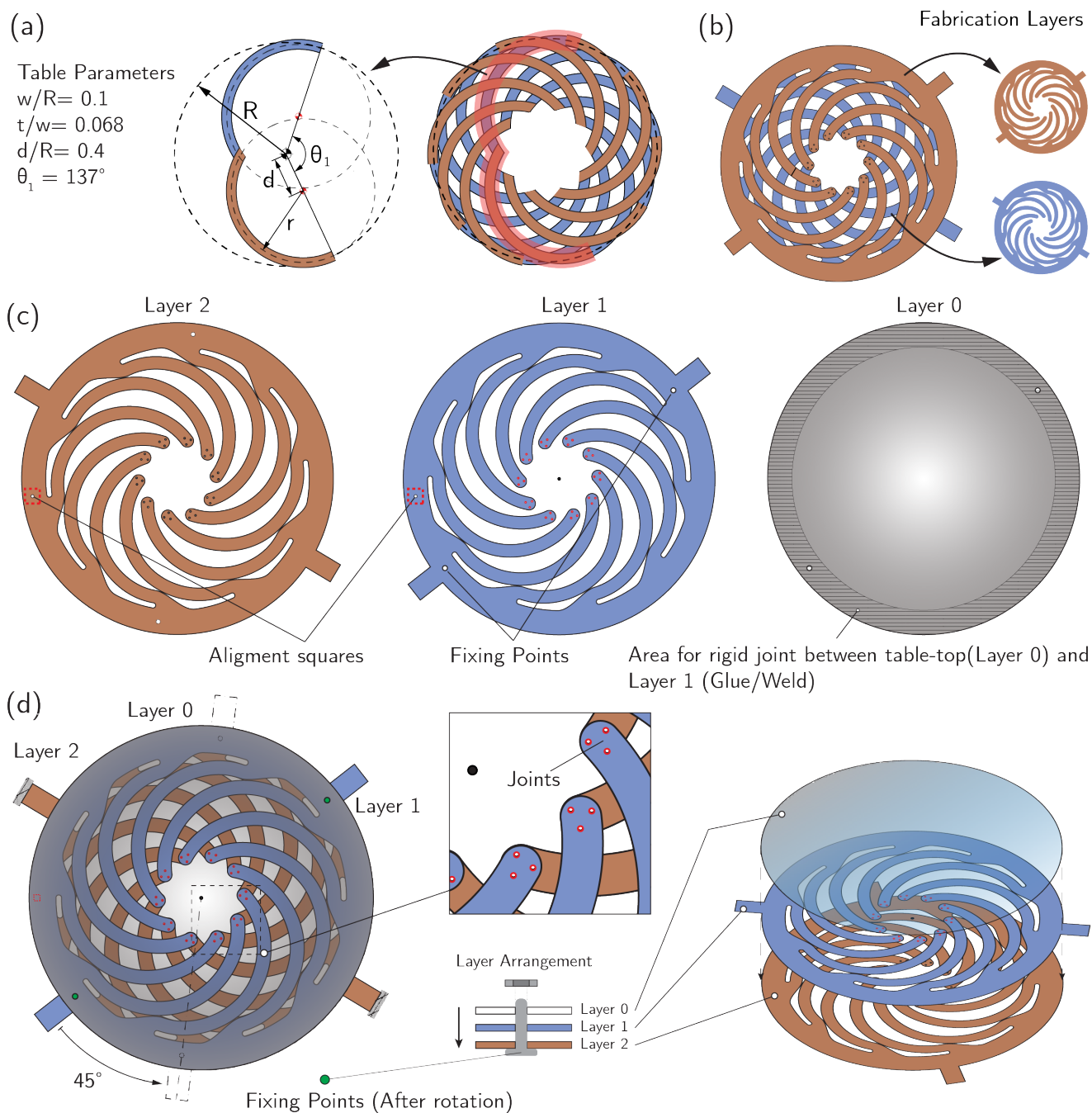
E. Deployable coffee table. The coffee table considered in Fig. 7 of the main text can be fabricated using the following steps (see Fig. S5):
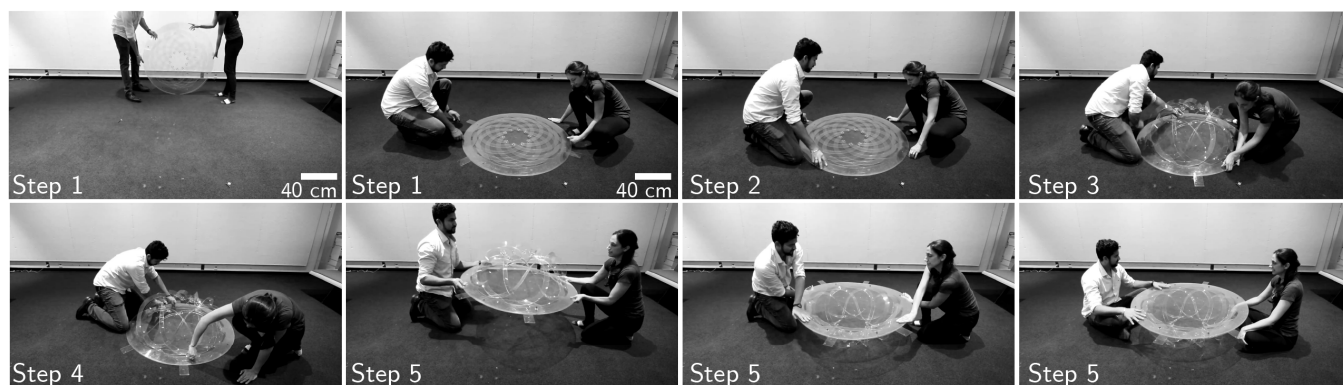
1. Cut a circular disc with a diameter of 1.14 m and the 2 parts shown in Fig. S5c out of 3/16" (4.76 mm) thick PETG plastic. The PETG is cut using the router module of the Zund Cutter. The 2 parts comprise 10 beams each and, when connected, form 10 double arc beams with $w/R = 0.1$, $t/w = 0.068$, $d/R = 0.4$, $\theta_1 = 137°$ and $R = 440.25$ mm.(Fig. S5a)

2. As shown in Fig. S5c, the table top (Layer 0) is glued/welded to the first layer of beams (Layer 1).

3. This assembly is then aligned with the other layer of beams (Layer 2) with the help of the alignment squares and the circular perimeter.

4. The pair of half beams are connected to each other using 3 pop-up rivets per beam (Fig. S5d).

5. The structure is placed on a flat surface with Layer 0 on the bottom and deployed. Then it is flipped and ready for use.

The coffee table can be deployed using the following steps (see Fig. S6):

1. Place the table in its compact and flat configuration on a flat surface with the tabletop (Layer 0) face down.

2. Ground the tabs of Layer 2 down with weight.

3. Rotate the tabs of Layer 1 in clockwise direction to deploy the table. Keep rotating until the 2 fixing points on opposite sides of Layer 1 (shown in green in Fig. S5d) align with those of Layer 2.

4. Using 2 pairs of nuts and bolts, fix Layer 1 to Layer 2 using the fixing points shown in green in Fig. S5b.

5. Flip the table in its upright position. It is ready for use.

6. The stability of the whole system can be increased by introducing a central tie between the ends of the beams or adding self-locking tabs on the beam, as shown in Fig. S7 for a centimeter-scale prototype.
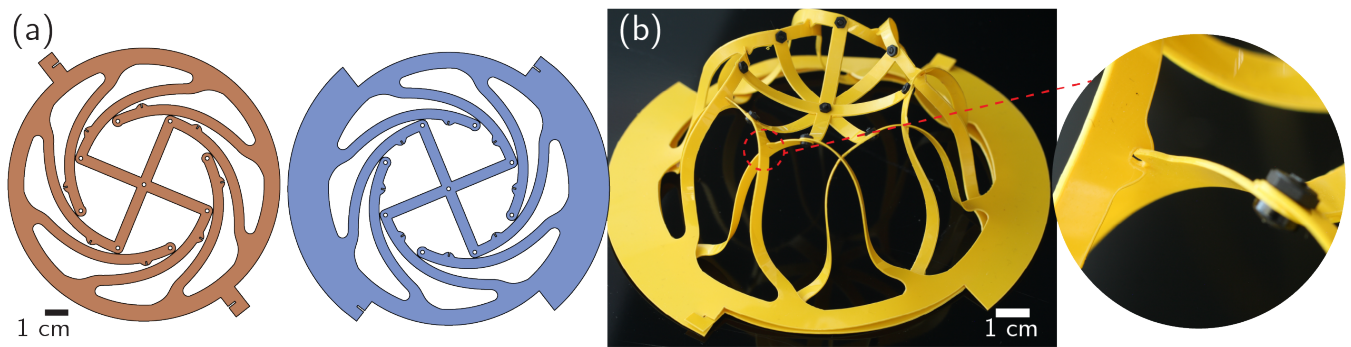
(a)

Table Parameters
w/R= 0.1
t/w= 0.068
d/R= 0.4
$\theta_1 = 137°$

R
θ_1
d
r

(b) Fabrication Layers

(c)

Layer 2

Layer 1

Layer 0

Aligment squares

Fixing Points

Area for rigid joint between table-top(Layer 0) and Layer 1 (Glue/Weld)

(d)

Layer 0

Layer 2

Layer 1

Joints

Layer Arrangement

Layer 0
Layer 1
Layer 2

45°

Fixing Points (After rotation)

Fig. S5. Deployable coffee table.(a) Parameters of our table (b) Table fabrication layers (c) Zoom in schematics of its 3 layers. (d) Schematics illustrating the joinery and assembly process.

Fig. S6. Deployment of our coffee table.

Saurabh Mhatre, Elisa Boatti, David Melancon, Ahmad Zareei, Maxime Dupont, Martin Bechthold, Katia Bertoldi

Fig. S7. (a) Self-locking tabs and a central tie are added to a centimeter-scale prototype of the table to increase its stability in the deployed configuration which proves to be an important revision for the next iteration of the table.(b) Detail view of self-locking tab
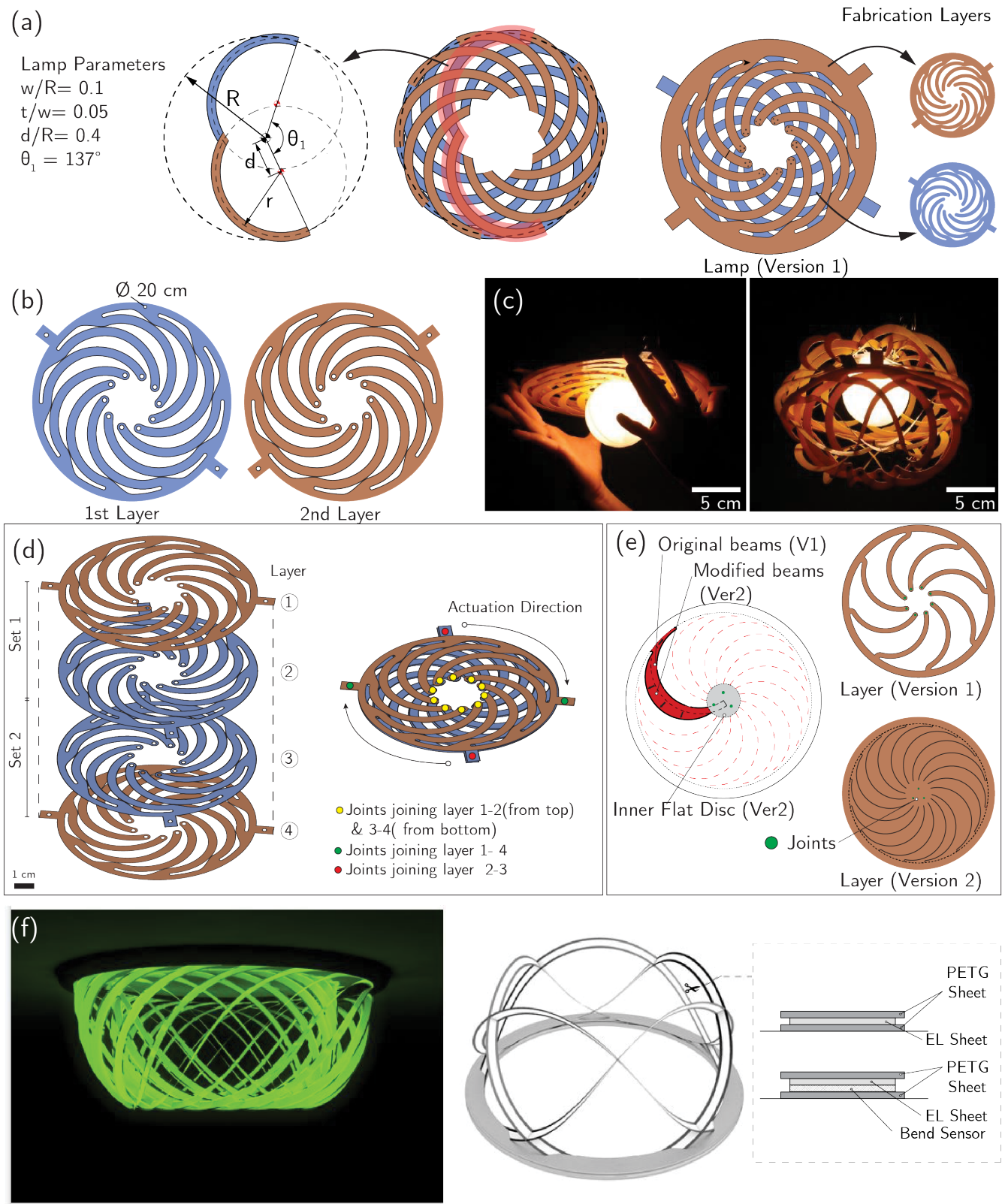
F. Lamp shade. The lamp shade considered in Fig. 8 of the main text can be fabricated using the following steps:

1. Laser cut the 2 parts shown in Fig. S8a out of 0.003 white PETG shims. Each disc comprises a chiral pattern with 16 curved cuts.

2. Connect 'Layer 1' to the fixed base of a turntable (McMaster Part No.1797K12) aligning the overlapping holes and using bolts and nuts.

3. Connect 'Layer 2' to the rotating part of the turntable.

4. Aligning the 3 holes in the center, fix 'Layer 1' and 'Layer 2' to each other using 3 M3 bolts/rivets to form 16 double arc beams with varying cross-section.

5. Connect the knob (shown in yellow in Fig. S8b) to the rotating part of the turntable, sandwiching 'Layer 2' in-between.

The lamp shade is deployed by rotating the knob clockwise to generate a relative motion between 'Layer 1' and 'Layer 2'. Finally, in Fig. S9 we report results for a lamp shade realized using circular arrays of curved beams with constant width. This layout exhibits large voids in both the flat and the expanded configuration, providing limited variations in shading.
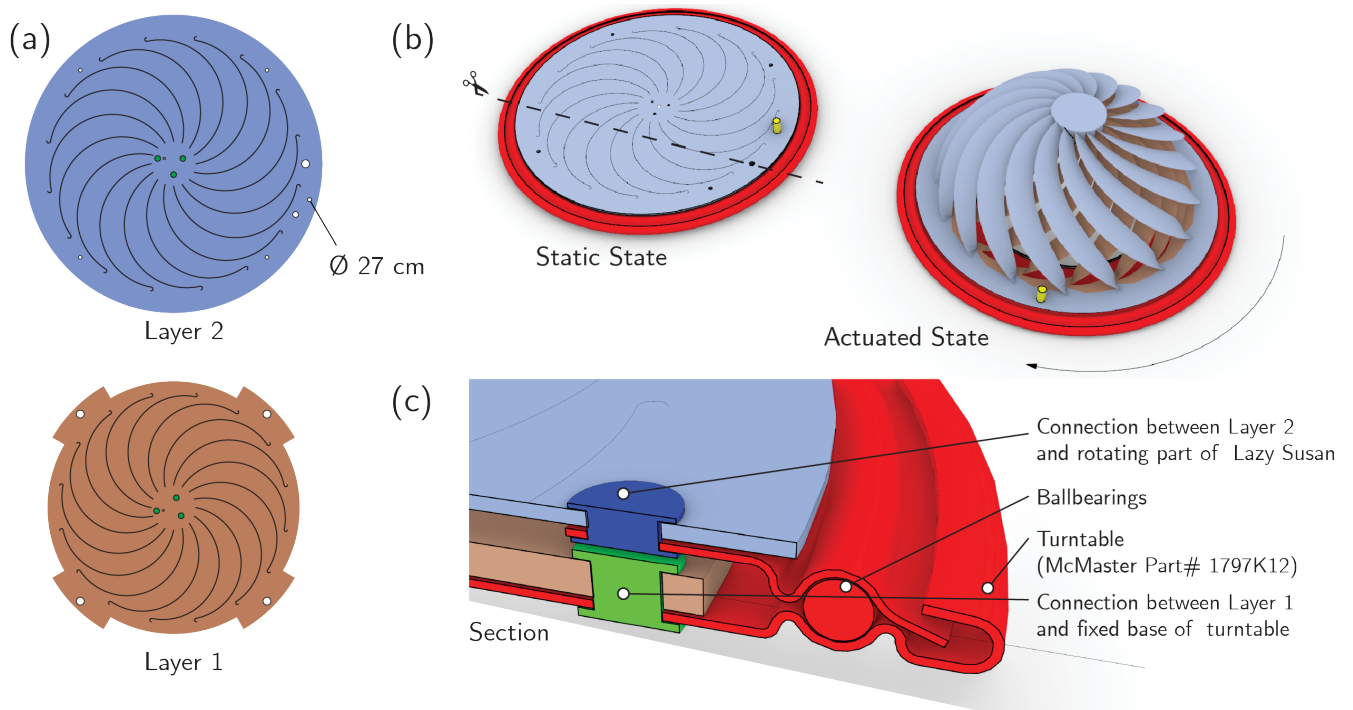
Fig. S8. Lamp shade. (a) Schematics showing its 2 parts. (b) Schematics showing the assembled lamp shade. (c) Sectional connection detail of the layers with the turntable

Saurabh Mhatre, Elisa Boatti, David Melancon, Ahmad Zareei, Maxime Dupont, Martin Bechthold, Katia Bertoldi

Fig. S9. Lamp shade realized using circular arrays of double arc beams. (a) Parameters of our design. (b) Schematics showing its 2 parts. The beams considered in this design are characterized by $w/R = 0.1$, $t/w = 0.05$, $\theta_1 = 137°$ and $d/R = 0.4$. (c) Snapshots of the lamp shade in its flat and deployed configuration. (d) Schematics showing details of the assembly process. (e) Schematics showing the changes made to the beams in order to reduce the void and form the lamp shade reported in Fig. 8 of the main text. (f) Snapshot of the deployed lampshade made out of electroluminicent film (left) and schematics showing the cross-section of the beams with the film and a a bend sensor for feedback. The flexible electroluminicent film glows when current passes through it and make the structure emit light in the deployed configuration.
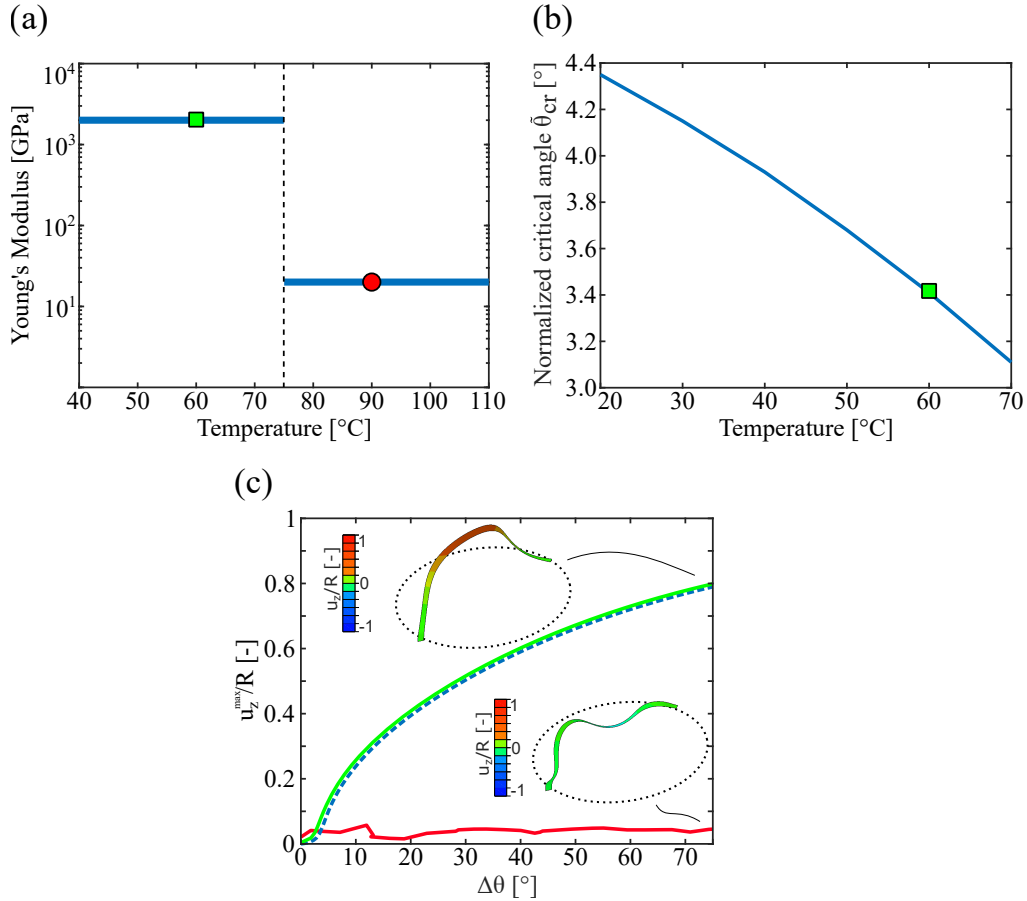
G. Metallic structures. Although all deployable structures reported in the main text were fabricated out of PETG sheet, any material can be used to realize the beam. As an example, metallic structures can be fabricated using the following steps (see Fig. S10):

1. Two sets of 6 fin layers (4 layers) are first laser-cut from a 0.025" thick sheet of *Easy-to-Form 1075 Spring Steel* .

2. One layer from each set is placed with the connection holes as reference and paired.

3. The layers are then connected using M1.2 mm bolts and nuts at 6 points as shown to form a set.

4. The independent sets are deployed to check for joint consistency.

5. Both the sets are aligned using the protruding tabs and are connected to each other. The central spirals of both sets are connected to each other using the same M1.2mm bolt and nut.

6. The 2 connected sets are deployed by rotating opposite facing tabs of one set towards the other to form a dome like structure.


Fig. S10. Snapshots of the 6 steps required for the fabrication of our structure out of *Easy-to-Form 1075 Spring Steel*.

Saurabh Mhatre, Elisa Boatti, David Melancon, Ahmad Zareei, Maxime Dupont, Martin Bechthold, Katia Bertoldi

S2. Additional results

(a)

(b)

(c)

Fig. S11. Effect of temperature. (a) Based on reported mechanical properties for PETG (1), we assume a constant coefficient of thermal expansion $\alpha = 1.2 \cdot 10^{-4} \, ^{\circ}C^{-1}$ and a step function for the Young's Modulus with $E = 2$ GPa for temperatures below the glass transition temperature $T_g = 75 \, ^{\circ}C$ and $E = 20$ MPa for temperatures above T_g. (b) Evolution of the critical buckling angle $\tilde{\theta}_{cr}$ as a function of temperature for a circular beam characterized by t/w=0.1, $w/R = 0.067$, $d/R = 0.4$ and $\theta_0 = 110^{\circ}$. The results indicate that an increase in temperature T leads to a small decrease in $\tilde{\theta}_{cr}$. Such small decrease of $\tilde{\theta}_{cr}$ can be attributed to the effective reduction of initial opening angle due to thermal expansion. (c) Effect of temperature on the post-buckling behavior of the circular beam. We find that the evolution of the maximum displacement u_z^{max}/R as a function of the opening angle $\Delta\theta$ for $T = 60 \, ^{\circ}C$ (green line) overlaps almost perfectly on the reference case at room temperature (blue dashed line). Differently, above the glass transition temperature (i.e. for $T = 90^{\circ}C$) the drastic change in Young's modulus largely affects the post-buckling behavior as the beam does not have enough bending stiffness to deform out of plane and the maximum displacement remains close to zero (red line).
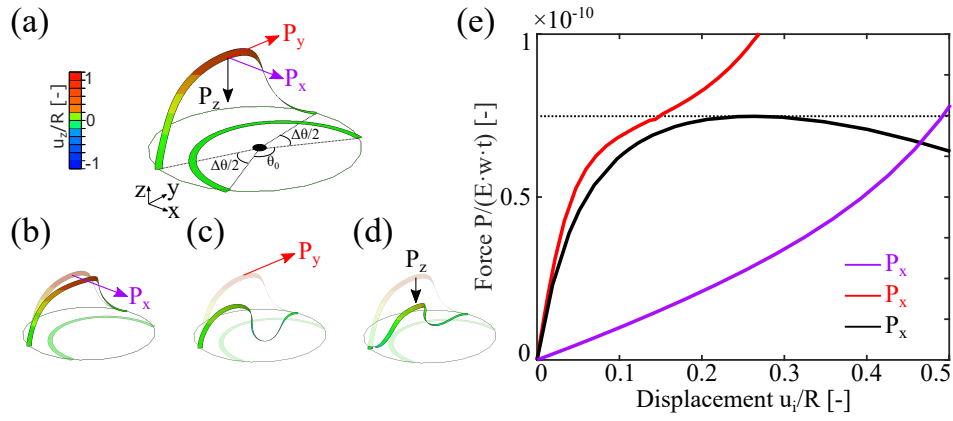
Fig. S12. Effect of applied forces. To clarify the effect of boundary forces (due to either environmental loads or externally applied forces) on our structures, we consider a concentrated force acting at the midpoint of a deployed circular beam characterized by t/w=0.1, $w/R = 0.067$, $d/R = 0.4$ and $\theta_0 = 110°$. (a) In our simulations, we first apply a rotation $\Delta\theta = 90°$ to deploy the beam and then apply a concentrated force along the (b) x, (c) y or (d) z direction, while maintaining the ends of the circular beam fixed. (e) Evolution of the normalized force, $P/(E \cdot w \cdot t)$, as a function of the normalized displacement in the direction of the applied force, u/R, for a concentrated force along the x (purple), y (red), and z (black) axis. We find that when the force is applied along the x or y direction, it increases monotonically with the midpoint displacement in the direction of the applied force, u. On the other hand, a force applied along the z-direction results in a local maximum in the force-displacement curve which corresponds to the onset of another buckling mode of the deployed beam. Note that if we consider a similar scale and material as the coffee table (i.e. $R = 500$ mm and $E = 2$ GPa), the peak force is ~16 N for this single beam.

     Saurabh Mhatre, Elisa Boatti, David Melancon, Ahmad Zareei, Maxime Dupont, Martin Bechthold, Katia Bertoldi

S3. Movies captions

Movie S1: Deployment of the structure considered in Fig. 1.
Movie S2: Deployment of the structure considered in Fig. 5.
Movie S3: Deployment of the structure considered in Fig. 6.
Movie S4: Deployable coffee table.
Movie S5: Lamp Shade.
Movie S6: Fabrication and deployment of metal structures.

References

1. Dupaix RB (2003) Ph.D. thesis (Massachusetts Institute of Technology).